Nanostructuring of a Polymeric Substrate with Well-Defined Nanometer-Scale Topography and Tailored Surface Wettability

Woo Lee, Mi-Kyoung Jin, Won-Cheol Yoo, and Jin-Kyu Lee*

School of Chemistry and Molecular Engineering, Seoul National University, Seoul 151-747, Korea

Received March 7, 2004. In Final Form: June 11, 2004

This study demonstrates a simple and highly reproducible method for fabricating well-defined nanostructured polymeric surfaces with aligned nanoembosses or nanofibers of controllable aspect ratios, showing remarkable structural similarity with interesting natural biostructures such as the wing surface of *Cicada orni* and the leaf surface of *Lotus*. Our studies on the present biomimetic surfaces revealed that the wetting property of the nanostructured surface of a given chemical composition could be systematically controlled by rendering nanometer-scale roughness. The nanofabricating method we developed can be readily extended to other thermoplastic polymeric materials (e.g., light-emitting polymers, conducting polymers, block copolymers, liquid crystalline polymers), and it could be applied to developing a new generation of optical and electronic devices.

Introduction

It has been well-established that material bulk properties such as mechanical friction, optical properties, and chemical and biological compatibility are substantially affected by the topography of a surface.[1] Most living creatures have known to fully exploit their novel surface structure for various functions.[2−5] For example, the lotus plant (*Nelumbo nucifera*) utilizes rough surface structure in the form of cilium-like nanostructures superimposed on micrometer-scale papillae to protect the leaf surface from harmful contaminants or parasites (rotus effect). With another example, geckos utilize millions of closely packed arrays of nanometer-sized setae on the surfaces of their feet in climbing up smooth vertical surfaces or in hanging from the ceiling. These unique surface functionalities of living systems are closely related to nanometer-scale surface topology, specifically cilia-like nanostructures. Therefore, the studies on this field could open up new perspective in the fabrication of various functional materials.[6,7] However, mimicking the biological surface topology is not simple and it often needs techniques beyond the limits of current technology; for practical applications of such bio-inspired surface topology, a convenient and simple method to fabricate surfaces over a substantial area is required first and foremost.

Here, we describe a simple method to generate large area bio-inspired polymeric surfaces with well-defined nanoembosses (nanolenses) or nanofibers of controllable aspect ratios. The key of the method is to use the electrochemically prepared nano-patterned aluminum sheet or nanoporous anodic aluminum oxide (AAO) as a replication template in the heat- and pressure-driven nanoimprint pattern transfer process (Figure 1). The method takes advantage of the unique tailoring capability of pattern sizes and heights of replication templates by simply varying the electrochemical parameters, which is not accessible in conventional lithographic techniques. Among other interesting surface properties expected, we first investigated the wetting property of these surfaces and demonstrated that the wettability of a hydrophobic polymer substrate could be systematically controlled from being merely hydrophobic to being super-hydrophobic by deliberately imparting nanometer-scale roughness on polystyrene (PS) substrates.

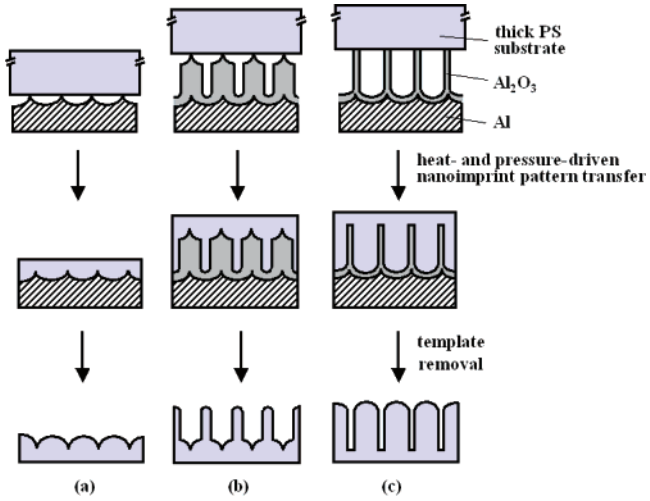

Figure 1. Schematic outline of the heat- and pressure-driven nanoimprint pattern transfer process for nanofabricating the surface of the thick polymer substrate with (a) aligned nanoemboss, (b) nanopost array with embossed base, and (c) aligned nanofibers.

Experimental Section

The replication templates used in our experiment were prepared by anodizing an aluminum sheet in oxalic acid (0.3 M $H_2C_2O_4$) according to the published route as follows.[8−10] Typically, surface-finished Al sheets were anodized under the constant

* To whom correspondence should be addressed. E-mail: jinklee@snu.ac.kr. Fax: +82-2-882-1080.

(1) Assender, H.; Bliznyuk, V.; Porfyrakis, K. *Science* **2002**, *297*, 973.
(2) Autumn, K.; Liang, Y. A.; Hsieh, S. T.; Zesch, W.; Chan, W. P.; Kenny, T. W.; Fearing, R.; Full, R. J. *Nature* **2000**, *405*, 681.
(3) Barthlott, W.; Neinhuis, C. *Planta* **1997**, *202*, 1.
(4) Gu, Z.-Z.; Uetsuka, H.; Takahashi, K.; Nakajima, R.; Onishi, H.; Fujishima, A.; Sato, O. *Angew. Chem., Int. Ed.* **2003**, *43*, 894.
(5) Ball, P. *Nature* **1999**, *400*, 507.
(6) Hiller, J. A.; Mendelsohn, J. D.; Rubner, M. F. *Nat. Mater.* **2002**, *1*, 59.
(7) Gleiche, M.; Chi, L.; Gedig, E.; Fuchs, H. *ChemPhysChem* **2001**, *2*, 187.

10.1021/la049411+ CCC: $27.50
Published on Web 08/06/2004

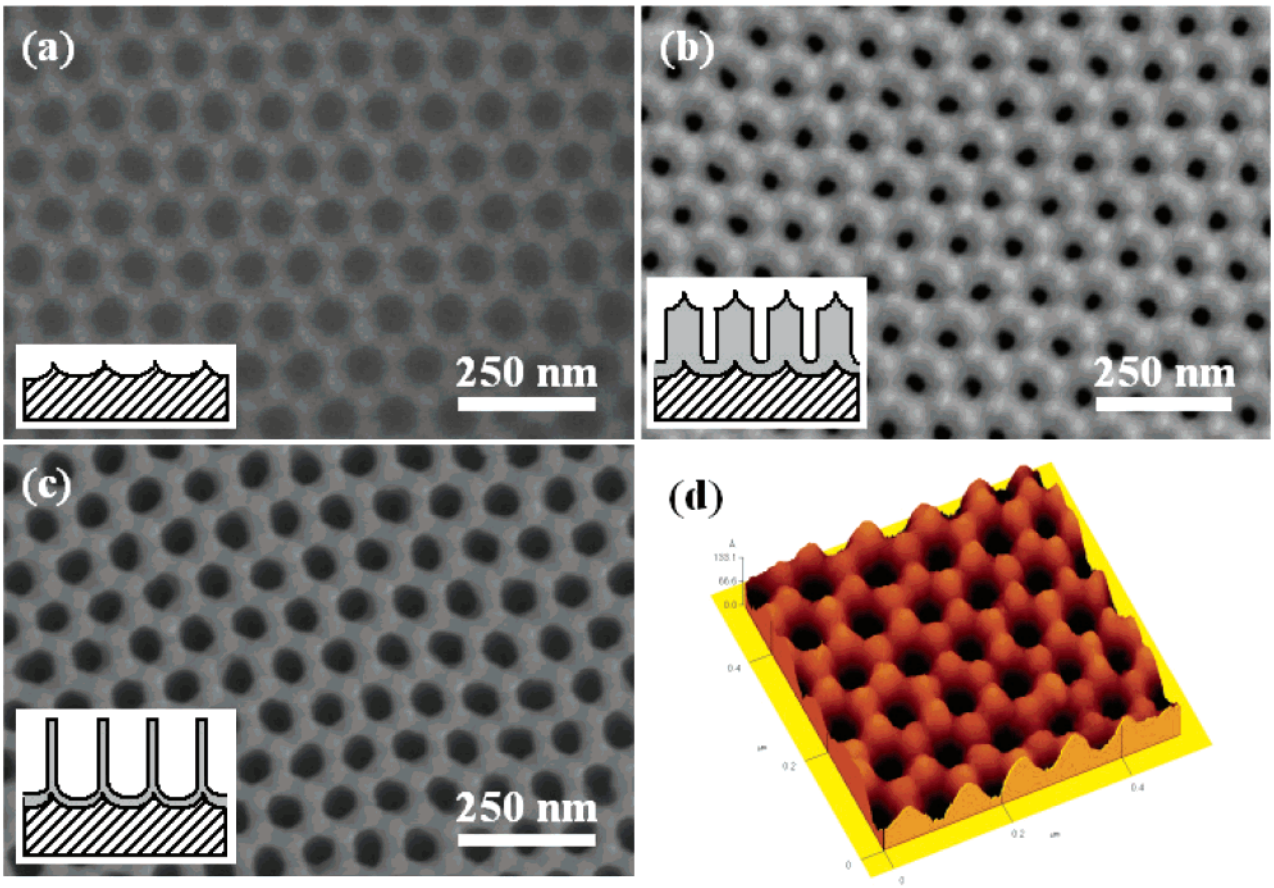

Figure 2. FE-SEM images of the replication templates: (a) textured aluminum, (b) as-prepared AAO, (c) pore-widened AAO. The schematic structures of each template are shown in the bottom-left inset of each micrograph. Topographic AFM image of textured aluminum is presented in part d.

cell voltages of 40 V for 17 h, using graphite cathodes. Subsequently, the porous oxide layer was completely removed by immersing the resultant films into the acid mixture of 1.8 wt % H_2CrO_4 and 6 wt % H_3PO_4 at 65 °C for 24 h to obtain a textured surface on the aluminum sheet. The resulting textured aluminum was thoroughly washed, dried, and then used as a replication template for the close-packed two-dimensional hexagonal array of polymeric nanoemboss. On the other hand, the replication templates for aligned PS nanofibers have been prepared by further anodizing the textured aluminum sheet at the same condition used in the first one. At this electrochemical condition, the microscopically determined pore diameter, pore density, and film growth rate turned out to be 40 nm, 1.0×10^{10} cm^{-2}, and about 10 μm/h, respectively. We could systematically adjust the pore diameters of the second anodized templates by wet-chemical etching using 5 wt % H_3PO_4 (34 °C). Under this wet-chemical etching condition, the pore diameter of the template increases at the rate of about 1 nm/min.

Whole area surface nanostructuring of the thick PS substrate was achieved by the nanoimprint pattern transfer technique, which is a modification of nanoimprint lithography and based on the heat- and pressure-driven impregnation of polymer melt into the nanopatterns of electrochemically prepared replication templates.[11−13] Replication templates were placed directly onto the PS substrate (typical size = 10 mm × 20 mm × 1 mm). A pressure was applied to hold the replication template against the PS substrate. The whole assembly was heated to a temperature (ca. 130 °C) well above the glass transition temperature of PS (T_g = 101 °C) to make the polymer chain sufficiently mobile for 5 min at an ambient atmosphere and then cooled to room temperature. After releasing the pressure, the replication template was removed from the polymer substrate by completely dissolving Al with saturated $HgCl_2$ solution and subsequently by immersing it into 6 wt % H_3PO_4 (40 °C) solution to give the large area, nanostructured PS surface. After that, the replicated sample was carefully washed with distilled water and allowed to air dry at room temperature. In the case of aligned PS nanofibers, the diameter of the PS nanofibers could be controlled by using the AAO replication templates with different pore diameters; the pore diameter was adjusted to the desired dimension by wet-chemical etching. On the other hand, the length of PS nanofibers could be controlled by appropriately varying the thickness of the AAO template (i.e., length of AAO nanochannels).

The morphology of the resulting nanostructured polymeric surfaces was investigated by a field emission scanning electron microscope (FE-SEM; Hitachi S-4300). The water contact angles of the nanostructured PS surfaces (typical sample dimension = 1×2 cm^2) were measured using the Krüs drop shape analysis system (G10/DSA10) at ambient temperature. The averaged advancing (θ_A) and receding contact angles (θ_R) were obtained by measuring for at least five separate drops on each sample surface by delivering/withdrawing distilled water with a microsyringe.

Results and Discussion

Figure 2a shows a typical FE-SEM image of the textured aluminum replication template, while Figure 2b,c displays two images of nanoporous aluminum oxide (AAO) with different pore diameters of 40 and 71 nm, respectively.

(8) Masuda, H.; Satoh, M. *Jpn. J. Appl. Phys.* **1996**, *35*, L126.
(9) Li, A. P.; Müller, F.; Birner, A.; Nielsch, K.; Gösele, U. *J. Appl. Phys.* **1998**, *84*, 6023.
(10) Lee, W.; Lee, J.-K. *Adv. Mater.* **2002**, *14*, 1187.
(11) Wang, J.; Sun, X.; Chen, L.; Zhuang, L.; Chou, S. Y. *Appl. Phys. Lett.* **2000**, *77*, 166.
(12) Behl, M.; Seekamp, J.; Zankovych, S.; Torres, C. M. S.; Zentel, R.; Ahopelto, J. *Adv. Mater.* **2002**, *14*, 588.
(13) Chou, S. Y.; Krauss, P. R.; Renstrom, P. J. *J. Vac. Sci. Technol., B* **1996**, *14*, 4129.

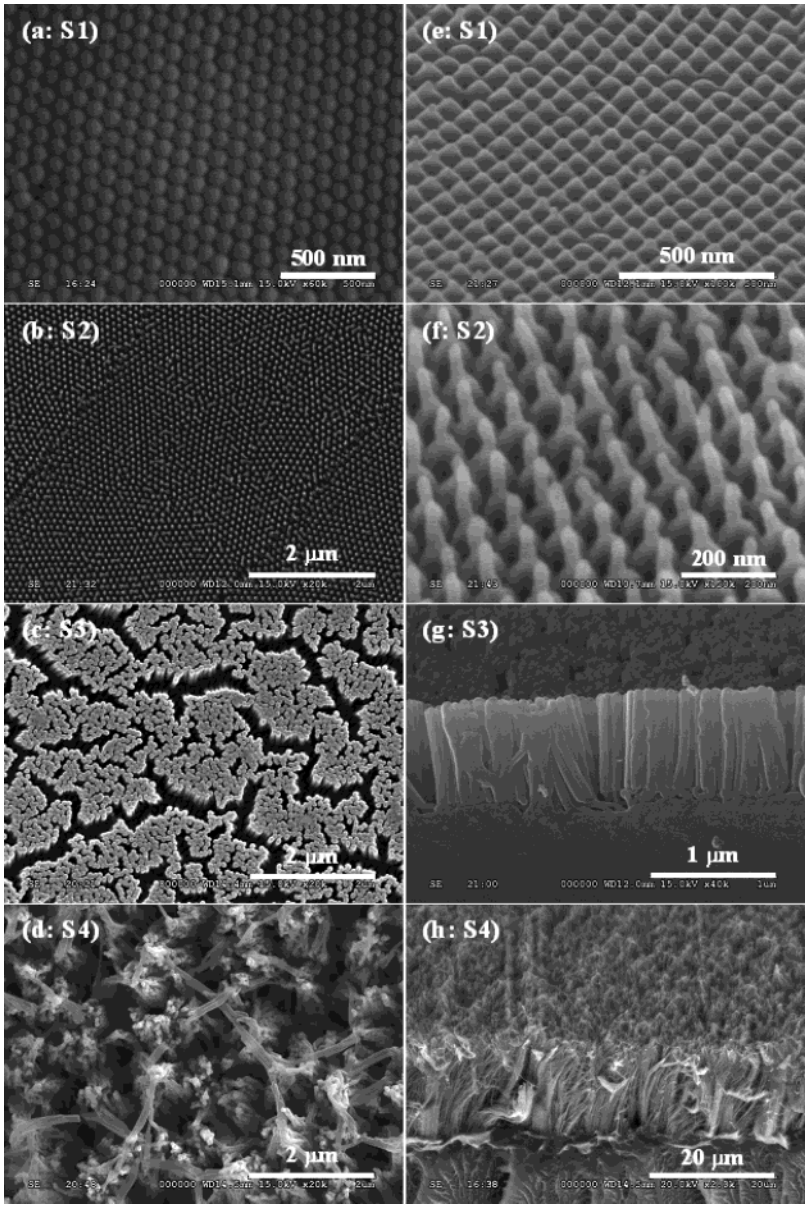

Figure 3. FE-SEM images of nanostructured PS surfaces: (a, S1) nanoemboss array, (b, S2) nanoposts array with embossed base, and aligned nanofibers (c, S3, and d, S4) with different lengths. The tilted or cross-sectional FE-SEM images of respective surfaces are presented in parts e−h.

The surface structure of textured aluminum is characterized as a close-packed hexagonal arrangement of approximately hemispherical concaves with the center-to-center distance of about 105 nm, in which each concave is surrounded by six distinct bumps as clearly seen from the topographic atomic force microscopy (AFM) image in Figure 2d. Anodization of textured aluminum produces highly ordered nanoporous AAO with cylindrical channels at the precise center of concaves without affecting the unique surface topography (Figure 2b). The channel length of AAO can be controlled by varying the anodization time. Controlled wet-chemical etching of the as-prepared AAO leads to an increase in the channel diameter concomitantly with leveling out the bumpy oxide surfaces (Figure 2c).

Figure 3 shows representative FE-SEM images of the nanostructured PS surfaces, along with tilted or cross-sectional images, replicated from the textured aluminum sheet (Figure 3a,e; S1), as-prepared AAO (Figure 3b,f; S2), and pore-widened AAOs with different thicknesses (Figure 3c,d,g,h; S3 and S4), respectively. Microscopic analyses using AFM and FE-SEM revealed that the density of surface nanofeatures for S1−S3 is exactly consistent with the pattern density ($\rho = 1.0 \times 10^{10}$ cm^{-2}) of the respective replication template, indicating high fidelity of the nanoimprint pattern transfer.[14] According to AFM sectional analyses on the surface S1, the average width and height of each emboss is estimated to be about 100 and 20 nm, respectively. From the cross-sectional FE-SEM analyses on the surface S2−S4, the average diameter of PS nanofibers was determined to be 40 nm for S1 and 71 nm for S3 and S4, which is in good agreement with the pore diameter of the replication templates. On the other hand, the observed length of nanofibers are about one-third smaller than the length of the nanochannel of the AAO replication templates. This indicates that the polymer

(14) The pattern density (ρ) of the replication templates was deduced from the average center-to-center distance (d; in nm) of the concaves (or the pores) in textured aluminum (or nanoporous AAO) using $\rho = [2/(3^{1/2}d^2)] \times 10^{14}$ cm^{-2}. For the surface S1−S3, the surface feature density could be estimated from the microscopic analyses. However, direct estimation for the density of PS nanofibers in the surface S4 could not be made because of severely distorted PS nanofibers.

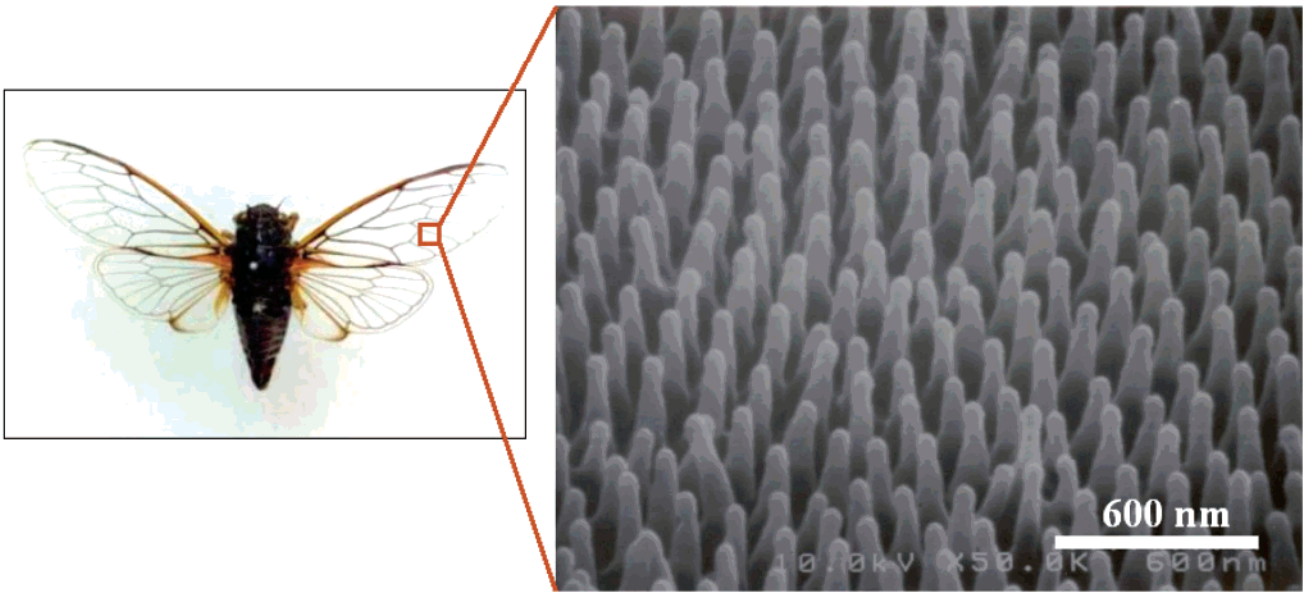

Figure 4. FE-SEM micrograph of the wing surface of *C. orni* with regularly aligned nanoposts.

melt does not completely fill the entire volume of nanochannels during the pattern transfer process. Such an incomplete filling could be attributed to the compressed air trapped between the advancing front of the polymer melt and the barrier oxide layer of a nanochannel. However, it is expected that incomplete filling can be overcome by performing nanoimprint pattern transfer under vacuum or by using a through-hole AAO replication template.

As manifested by the present micrographs, the overall surface topography is significantly affected by the aspect ratio (length divided by diameter) of the surface nanofeatures. The surfaces (S1 and S2) comprised of nanoemboss or nanofiber with a small aspect ratio exhibit nearly perfect hexagonal arrangement of the surface nanofeatures, as shown in Figure 3a,b. On the other hand, we could not observe any perfect hexagonal arrangement of individual nanofibers for the surface S3 and S4, which is expected from the hierarchically organized channel structure in the AAO replication template. As the aspect ratio increases, the aligned nanofibers form into bundles and develop submicrometer-sized valleys as presented in Figure 3c. Such a morphological evolution can mainly be attributed to the flexible nature of polymeric nanofibers having a large surface area, which results in strong interactions between the nanofibers during the processes of removal of the alumina replication template and the subsequent sample drying. This effect influences rather strongly on the overall surface morphology of aligned PS nanofibers, because the aspect ratio of nanofibers increases further. As shown in Figure 3d, individual PS fibers are severely deformed to produce a twisted bundle and cannot stand upright well on the polymer substrate resulting in a three-dimensionally rough surface. In fact, we have found that similar morphological evolution also emerges even in case of the metallic nanowires, which are mechanically much more rigid compared with polymeric nanofibers.

As was mentioned, the surface structure has significant biological importance in living creatures. The rough surface microstructure can function as an effective means of minimizing the adhesion between contaminating particles (or harmful chemicals) and biological surfaces. In addition, such a roughness in biological surfaces even provides water-repellent characteristics, enabling the

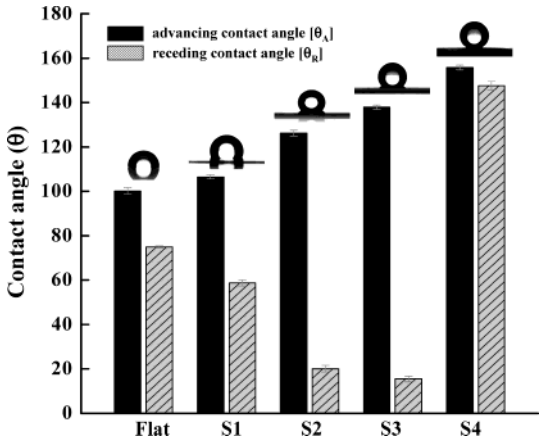

Figure 5. Advancing and receding water contact angle of nanostructured PS surfaces, together with the contact angle of the flat PS surface (flat). The shape of a water droplet placed on the each surface is presented as an inset.

living creatures to be freed from harmful organic contaminants or parasites (i.e., self-cleaning ability).[3]

It is worthy to note here that the surface S2 with a periodic array of nanoposts with embossed bases shows remarkable structural similarity with the wing surface of *Cicada orni*, who maintains flight capability by effectively removing dust particles from its wing surface by virtue of minimized interfacial interaction between dust particles and the surface of the wing with regularly sculptured nanostructure (Figure 4).[3,15] On the other hand, the surfaces S3 and S4 with aligned PS nanofibers exhibit some structural analogies to those of naturally occurring super-hydrophobic surfaces, where needlelike surface features prevent strong attachment of water droplets onto the surfaces.[3,16]

To get the knowledge of dynamic wetting characteristics of the samples, we have measured the advancing/receding water contact angle (θ_A/θ_R) and estimated the contact angle hysteresis ($\Delta\theta$). Figure 5 shows the advancing and receding contact angle data for the smooth PS substrate and the

(15) Wagner, T.; Neinhuis, C.; Barthlott, W. *Acta Zool. (Stockholm)* **1996**, *77*, 213.

(16) Feng, L.; Li, S.; Li, Y.; Li, H.; Zhang, L.; Zhai, J.; Song, Y.; Liu, B.; Jiang, L.; Zhu, D. *Adv. Mater.* **2002**, *14*, 1857.

surfaces S1−S4, together with the shape of a water droplet on the respective surfaces. In the figure, the difference between the advancing and the receding contact angle corresponds to the contact angle hysteresis of the surface. Advancing (θ_A) and receding (θ_R) water contact angle values on a flat PS film were $100.2 \pm 1.4°$ and $75.0 \pm 0.5°$, respectively. As clearly seen from the figure, the advancing contact angle (θ_A) increases systematically as the surface roughness increases. On the other hand, the surfaces S1−S3 show pronounced contact angle hysteresis. These surfaces exhibit a high advancing contact angle (θ_A) but very low receding contact angles (θ_R), even compared with the flat PS surface. A typical water drop (ca. 1.5 mm in diameter) placed on these samples came to rest on the surfaces and did not roll off even when the samples were tilted until vertical. On the contrary, the surface S4 shows superhydrophobic surface property with low contact angle hysteresis; $\theta_A/\theta_R = (155.8 \pm 1.1°)/(147.6 \pm 1.9°)$. A water drop placed on the surface rolls easily on the horizontal surface upon slight tilting, reflecting the high degree of water-repellent surface property.

The observed wetting behavior of the present nanostructured surfaces could be understood in terms of contact line structure formed at the interfaces between solid, liquid, and air.[17−22] For the surfaces S1−S3, it is expected that solid−liquid contact lines on these surfaces are very smooth and stable because of the almost same height of the surface nanofeatures, although in-plane contact lines are somewhat tortuous. It is also expected that a water droplet placed on the surfaces will collapse over the surface nanofeatures probably because of the droplet weight, resulting in effective intrusion of water into the surface nanofeatures. In this case, the contract interface will be solely solid−liquid with a thermodynamic equilibrium energy. The movement of the contact line requires a force to overcome the energy barrier (i.e., the interaction energy) formed by a solid−liquid interface at the advancing or receding front; this energy barrier is the origin of contact angle hysteresis.[17,22,23] For the surface systems where effective water intrusion occurs, the contact angle hysteresis increases as the surface roughness increases, because the contact interface area increases owing to the increase in surface roughness (i.e., Wenzel's hydrophobicity mode).[24] Therefore, the observed systematic increase in contact angle hysteresis in the surfaces S1−S3 could be understood as a result of increase in the surface roughness, whereas a quite different contact line structure could be emerged from the surface S4, of which the peak-to-peak roughness is much greater than those of the surfaces S1−S3. Contact lines on such a randomly rough surface are expected to be contorted and extremely unstable, preventing water from intruding into interfiber spaces. Namely, large peak-to-peak roughness can serve as an effective means of trapping sufficient air to give the composite surface effect (i.e., Cassie and Baxter's hydrophobicity mode).[25] Accordingly, the present experimental results suggest that a proper interval or height difference in the surface nanofeatures is prerequisite to achieve the superhydrophobic wetting property for a surface with nanometer-scale roughness.

Conclusions

In summary, we have shown a simple and highly reproducible method for the fabrication of well-defined nanostructured polymeric surfaces with aligned nanoembosses or nanofibers of controllable aspect ratio and exemplified that the wetting property of the nanostructured surface could be systematically controlled by rendering nanometer-scale roughness. Because the nanostructuring method described above can be readily extended to other thermoplastic polymeric materials (e.g., light emitting polymers, conducting polymers, block copolymers, liquid crystalline polymers), it can be anticipated that the method could be applied to developing a new generation of optical and electronic devices. From the viewpoint of controlling surface roughness, it is also expected that the present study could provide a good basis for designing many other functional nanostructured surfaces: antireflection surfaces, optically transparent superhydrophobic surfaces, biologically compatible surfaces, and and so forth.

Acknowledgment. This work was supported by a grant from the National R&D Project for Nano Science and Technology of the KISTEP. W.-C.Y. is grateful for the award of a BK21 fellowship.

LA049411+

(17) Öner, D.; McCarthy, T. J. *Langmuir* **2000**, *16*, 7777.
(18) Li, S.; Li, H.; Wang, X.; Song, Y.; Liu, Y.; Jiang, L.; Zhu, D. *J. Phys. Chem. B* **2002**, *106*, 9274.
(19) Miwa, M.; Nakajima, A.; Fujishima, A.; Hashimoto, K.; Watanabe, T. *Langmuir* **2000**, *16*, 5754.
(20) Yoshimitsu, Z.; Nakajima, A.; Watanabe, T.; Hashimoto, K. *Langmuir* **2002**, *18*, 5818.
(21) Extrand, C. W. *Langmuir* **2002**, *18*, 7991.
(22) Chen, W.; Fadeev, A. Y.; Hsieh, M. C.; Öner, D.; Youngblood, J.; McCarthy, T. J. *Langmuir* **1999**, *15*, 3395.
(23) Wolfram, E.; Faust, R. In *Wetting, Spreading and Adhesion*; Padday, J. F., Ed.; Academic Press: London, 1978; p 213.
(24) Wenzel, R. W. *Ind. Eng. Chem.* **1936**, *28*, 988.
(25) Cassie, A. B. D.; Baxter, S. *Trans. Faraday Soc.* **1944**, *40*, 546.